Materials Research Proceedings 41 (2024) 723-732 https://doi.org/10.21741/9781644903131-80

Investigation of heat transfer dependencies in quenching of extrusion profiles based on experiment and FEM simulation

KNIAZKIN Ivan[1,a *], KRYLOV Vladimir[1,b], SHITIKOV Andrei[1,c], KULAKOV Ivan[1,d], BIBA Nikolay[1,e]

[1]Micas Simulations Limited, Temple Court, 107 Oxford Road, Oxford, OX4 2ER, United Kingdom

[a]ivanknjazkin@gmail.com, [b]krylov@qform3d.com, [c]a.a.sh.ggml@gmail.com, [d]kulakov@qform3d.com, [e]nick@qform3d.com

Keywords: Quenching, Aluminium, Qform, Extrusion, Heat Transfer, Spray Cooling, Cooling Rate

Abstract. The objective of this study is to establish a comprehensive method, devoid of computational fluid dynamics (CFD) calculations, for determining the surface heat transfer coefficient during spray cooling. This technique enables the derivation of the heat transfer coefficient's dependence on the temperature of the cooled surface by utilizing known data regarding the number, relative positioning, and catalog characteristics of nozzles. Additionally, adjustable parameters of the quenching system such as the pressure and flow rates of water and air are considered in the methodology. Implemented within the commercial finite element (FE) package QForm UK, this technique is validated using independent experimental data that faithfully replicates real production conditions encountered during the quenching of extruded profiles made from aluminum alloys.

Introduction

Controlling extrusion parameters is crucial to produce precise, high-quality aluminum profiles with specific dimensions and mechanical properties. The goal is to create defect-free profiles within tight tolerances, ensuring acceptable material properties and increased productivity. Post-extrusion treatments like quenching and aging are essential for achieving the desired product strength, especially since most profiles are made from heat-treatable aluminum. At the same time, quenching itself may cause some shape and surface imperfections, especially in case of water-based methods [1].

The choice of quenching method significantly affects the final properties of profiles. Here, advanced cooling simulations play a vital role in optimizing quenching processes, contributing to improved profile uniformity and superior mechanical properties. However, to effectively utilize the simulation engine and derive meaningful results, it is imperative to incorporate reliable inputs crucial for simulating the quenching process. Among these inputs, the heat transfer coefficient plays a pivotal role in defining the temperature evolution within the profile during cooling. The dependency of the heat transfer coefficient on the surface temperature of the profile and liquid flux density profoundly influences the accuracy of simulation and the subsequent applicability of the software in an industrial setting.

Integrating simulation techniques with practical applications enhances the precision and efficiency of manufacturing heat-treatable aluminum alloy profiles [2]. Numerous studies have focused on the quenching of aluminum profiles [3]-[5]. However, the literature concerning numerical simulations of quenching processes in profile extrusion is notably limited, with only a few works available [1, 6, 7].

Description of the Case Study

Researchers in [8] conducted an experiment to track temperature changes along a treated profile during cooling. They used a spray cooling device on a separate roller conveyor system, eliminating the need for attachment to the press line. To replicate industrial cooling conditions, an electric resistance furnace and forced air circulation mechanism were set up (Fig. 1).

The cooling system included water and air elements, housed in a frame with two holders, each equipped with 30 nozzles. These nozzles were evenly spaced at 56 mm intervals in a vertical arrangement (Fig. 2). Maintaining a fixed distance of 100 mm between the nozzle exit and the profile surface, water and air pressures were controlled within a range of ±0.05 bar from their set values.

Fig. 1. Water-air cooling installation: 1 – furnace; 2 – roller conveyor; 3 – frame; 4 - holder with nozzles; 5 – guides; 6 - sample with installed thermocouples [8]

The profiles used in the experiment were EN AW-6060 aluminum alloy with a 20x40 mm rectangular cross-section. Samples were moved using a cable wound around a drum connected to a motor shaft, allowing rotational speeds from 7 to 84 rpm and linear velocities from 2 to 24 m/min, covering typical extrusion speeds.

In this study, the one of the main focuses was on simulating the described process. The aim was to determine convective boundary conditions in such a way that the computed cooling curve aligns with the curve obtained from a thermocouple placed at the center of the sample during cooling in laboratory tests conducted under industrial conditions.

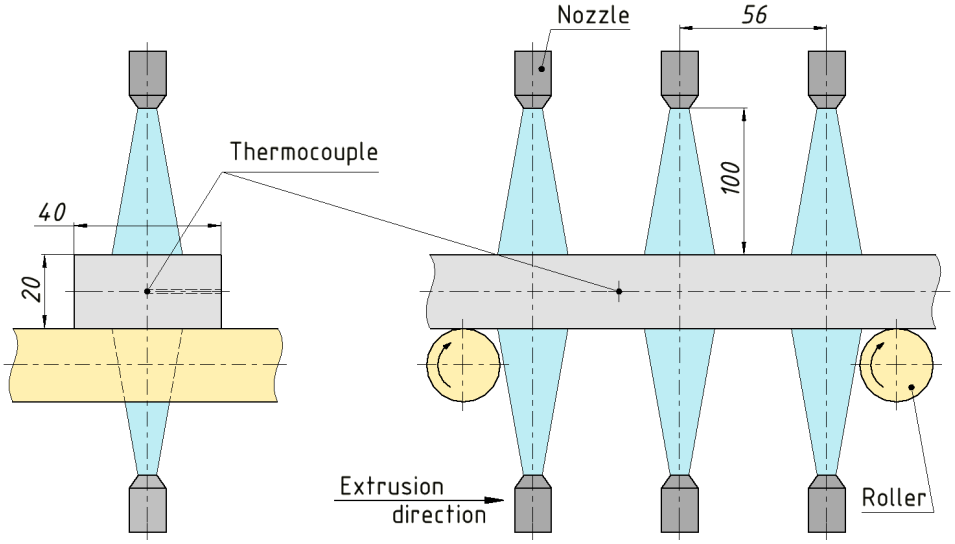

Fig. 2. Rescaled scheme of the investigated cooling process [8]

Description of the Parameters and Algorithms Used in the Simulation

The simulation was performed using a specialized module in the QForm UK FEM software, designed specifically for simulating quenching with various conditions and cooling systems, including water spraying. The technological parameters used in simulation are detailed in Table 1.

Table 1. Technological parameters of the process used in simulation

Mode name	p_{water} [bar]	p_{air} [bar]	$V_{profile}$ [m/min]	$T_{initial}$ [°C]
W3A3-3	3	3	3	545
W5A3-3	5	3	3	539
W5A3-6	5	3	6	539

The study detailed in article [8] utilized full-cone water-air nozzles, specifically SU12 from Spraying Systems Co. These nozzles consist of two components: the fluid cap 2850 and the air cap 73160. As outlined in the catalog [9], the spray angle falls within the range of 12-15 degrees (considered equal to 15 degrees for simulation), with the orifice equivalent diameter measuring 0.71 millimeters (converted from inches).

During the cooling process using sprayers, the efficiency of heat transfer is contingent upon the distance between the surface undergoing cooling and the nozzle of the sprayer (Fig. 3). The liquid flux density diminishes along the spray axis of the spraying jet, decreasing from its maximum value (q_{max}) at the nozzle exit to zero (Fig. 3b). Additionally, an uneven distribution is observed in the cross-section of the jet, wherein the highest flux density in a specific section of the jet, defined by z coordinate, decreases from q^z_{max} at the center to zero at the boundary (Fig. 3a). To incorporate the spatial dependency of the heat transfer coefficient, relative distribution functions η_r and η_z are introduced in this study.

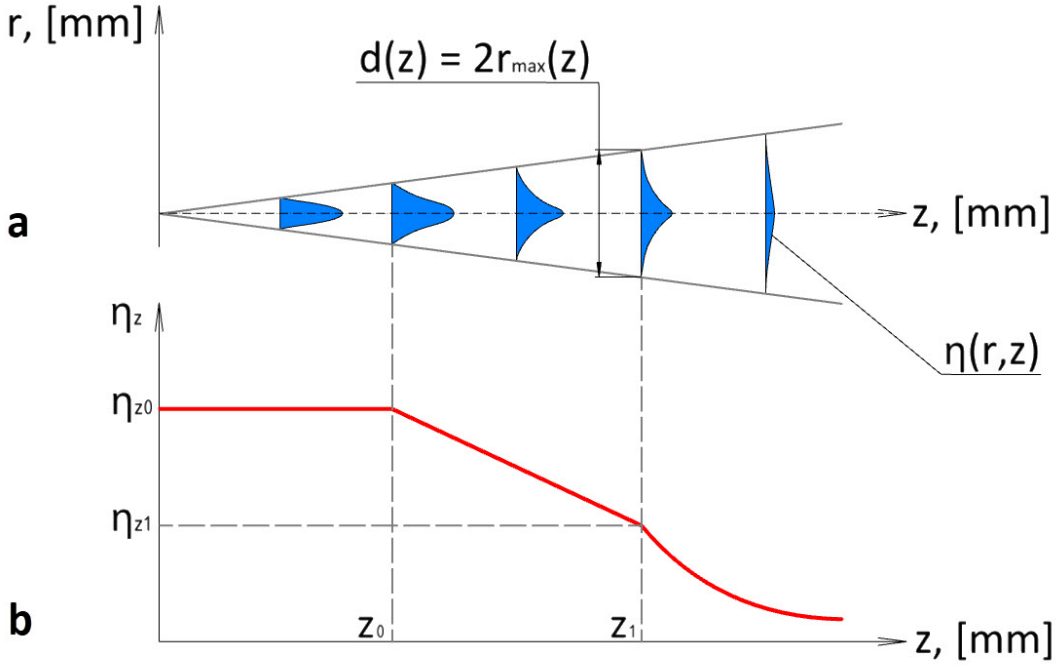

Fig. 3. Distribution of heat transfer intensity: a – in the cross-section; b – along the spraying jet by distance from nozzle

Materials Research Proceedings 41 (2024) 723-732 https://doi.org/10.21741/9781644903131-80

Relative liquid flux in spray cross cut. In QForm UK, it is assumed that relative liquid flux in spray cross cut is expressed using the following dependence [10, 11]:

$$\eta_r(r) = \frac{q_r^z}{q_{max}^z|_{r=0}} = \left[1 - \left(\frac{r}{r_{max}}\right)^{\frac{3}{2}}\right]^2 \quad (1)$$

Here r – relative distance from axis of symmetry of the jet to the cross-section point, r_{max} – maximum radius of the cross section of the jet. Graphical representation of this dependence is presented in Fig. 3a.

The average value of the relative distribution function across the cross section of the jet can be calculated using the following formula:

$$\bar{\eta}_r = \frac{2\pi \int_0^{r_{max}} \eta_r(r) r dr}{\pi r_{max}^2} \quad (2)$$

Relative liquid flux by distance from nozzle. Relative liquid flux by distance from nozzle can be described with the following system of equations:

$$\eta_z(z) = \frac{q_{max}^z}{q_{max}|_{z=0}} = \begin{cases} \eta_{z0}, & z \le z_0 \\ \eta_{z0} - \dfrac{\eta_{z0} - \eta_{z1}}{z_1 - z_0} \cdot (z - z_0), & z_0 < z \le z_1 \\ \eta_{z1} \cdot \left(\dfrac{z_1}{z}\right)^n, & z_1 < z \end{cases} \quad (3)$$

z – distance from the nozzle exit to the cross section of the jet, the section from z_0 to z_1 indicates the linear velocity decrease, $> z_1$ – section of nonlinear decrease in jet velocity [10, 11]. Graphical representation of this dependence is shown in the Fig. 3b.

Thus, an expression can be derived to determine the surface density of the liquid flux at any specified point within the local coordinate system of the spraying jet:

$$q(z,r) = \frac{4 \cdot Q}{\pi \cdot d(z)^2} \cdot \eta_z(z) \cdot \frac{\eta_r(r)}{\bar{\eta}_r} \quad (4)$$

The variable $Q = f(p_w, p_a)$ represents the dependence of liquid flow rate through the nozzle on water pressure and air pressure, as provided in the catalog [9].

Derivation of Heat Transfer Relationships

Regrettably, in the laboratory setup described in [8], all sprayers are positioned equidistant from the surface of the cooled profile. Consequently, it is not feasible to verify the parameters of the function η_z based on the data provided in [8]. Therefore, in subsequent calculations, it is assumed that η_z remains constant at a value of 1.

In a general context, the heat transfer coefficient is contingent on both the liquid flux density and the temperature of the cooled surface. Utilizing the insights from reference [12], the following expression can be proposed to represent the dependence of the surface heat transfer coefficient on liquid flux density and surface temperature:

$$HTC(q,T) = \overline{HTC}(q) \cdot \xi(T) \quad (5)$$

In this equation, $\overline{HTC}(q)$ denotes the mean heat transfer coefficient averaged over total surface temperature range. The parameter ξ represents the ratio of the heat transfer coefficient at a specific temperature to the average heat transfer coefficient across the entire temperature range as a function of the surface temperature [12]. Its graphical depiction is presented in Fig 4.

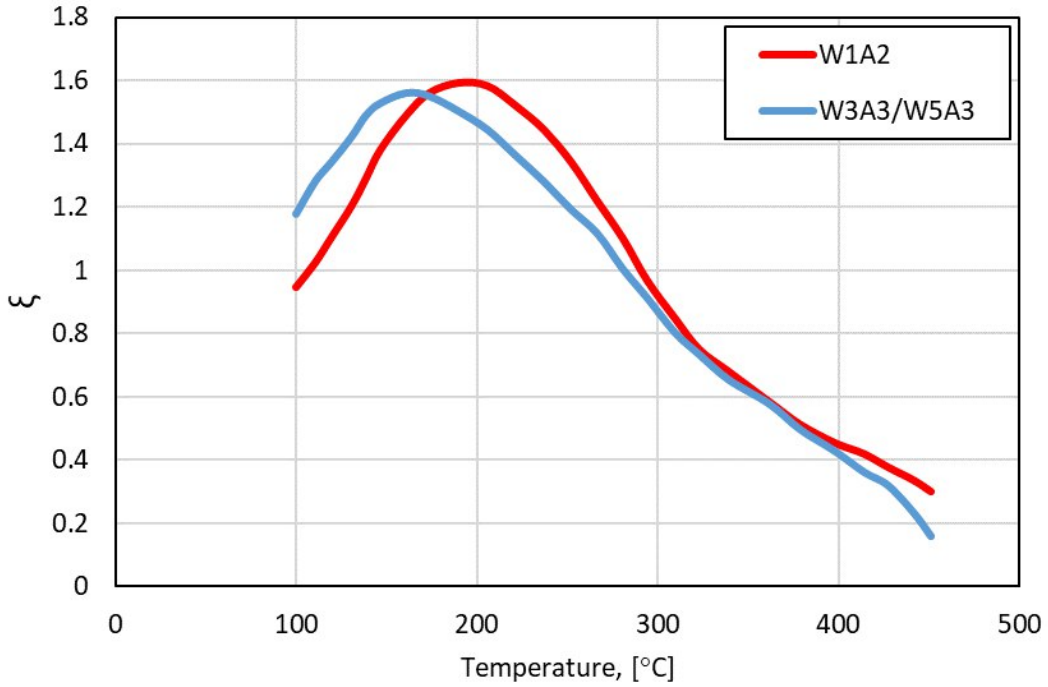

Fig. 4. Dependence of the relative heat transfer coefficient on temperature for the investigated spray parameters

Derivation of the Dependence of HTC on Liquid Flux Density. To establish a dependency in the form of $\overline{HTC} = f(q)$, the surface liquid f density values were determined for each combination of cooling modes explored in the study outlined in the work [8] in the following form:

$$q_{w_i a_i} = \frac{4Q_{w_i A_i}}{\pi d (z^*)^2} \tag{6}$$

Here, $Q_{w_i A_i}$ – liquid flow rate for the certain cooling mode, $d = f(z)$ represents the cross-sectional diameter of the jet at a given distance z from the nozzle, and $z^* = 100$ mm signifies the distance from the nozzle to the cooled surface in the experimental setup depicted in Fig. 2.

Unfortunately, the catalog [9] for the Spayer Systems nozzle model used in experiment lacks the required water flow rates for modes W1A2 and W5A3, essential for establishing the functional relationship, along with mode W3A3. To address this gap in information, a regression was constructed using available values, followed by extrapolation. Table 2 provides the derived values for the liquid flux density for the relevant combinations.

Table 2. Liquid flux density for different cooling modes

Cooling mode	W1A2	W3A3	W5A3
q, L/(min · m^2)	124	415	967

Hence, to characterize the dependence of the $\overline{HTC}$ on the determined liquid flux density values, a power-law regression was employed:

$$\overline{HTC}(q) = 0.425q^{0,533} + 1.456 \tag{7}$$

This dependence is graphically represented on Fig. 5.

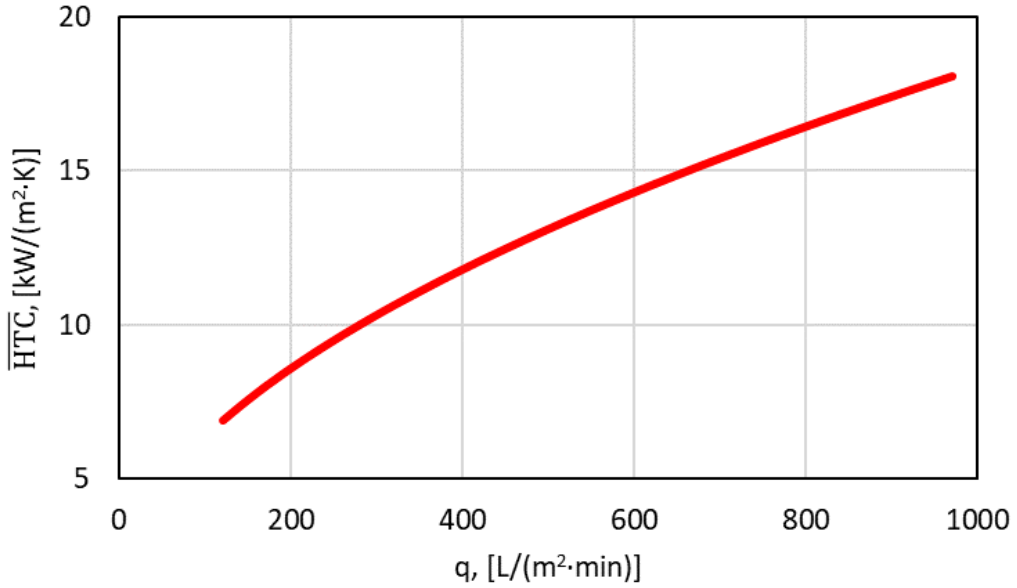

Fig. 5. Dependence of the heat transfer coefficient averaged over total temperature range on liquid flux

Fig. 6 represents the resulting dependence of heat transfer coefficient on temperature which was additionally extrapolated to the working temperature of extrusion process.

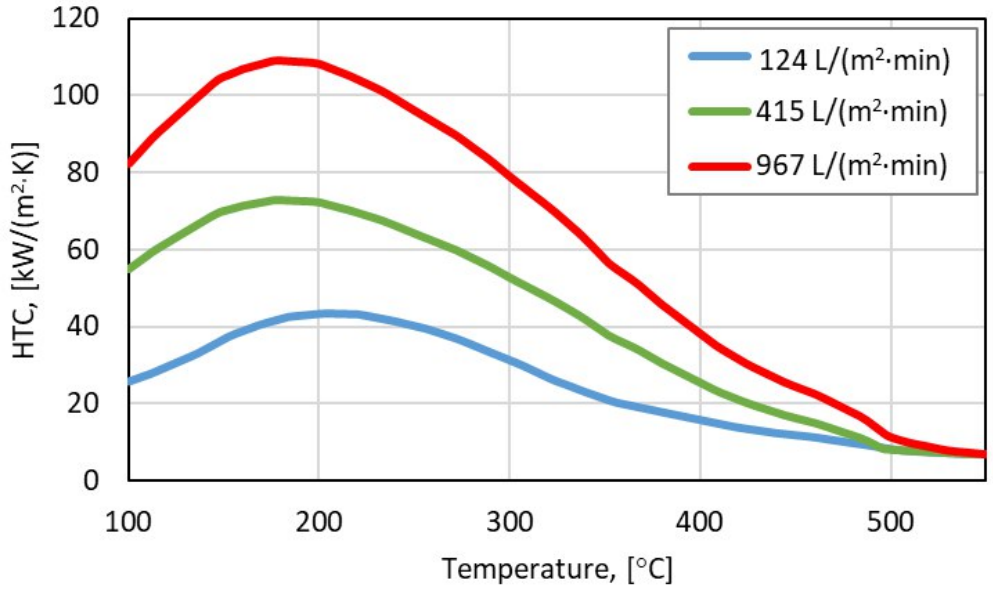

Fig. 6. Dependence of the heat transfer coefficient on temperature

Results and Discussion

Fig. 7 presents the simulation outcomes, illustrating different phases of the process and providing a visual representation of the simulation setup along with the arrangement of the nozzles. The initial temperatures of the profile were set at 545°C, 539°C, and 539°C, respectively, in alignment with the data reported in [8]. This accounts for the temperature variation as the sample progresses from the furnace to the table immediately before entering the designated quenching station.

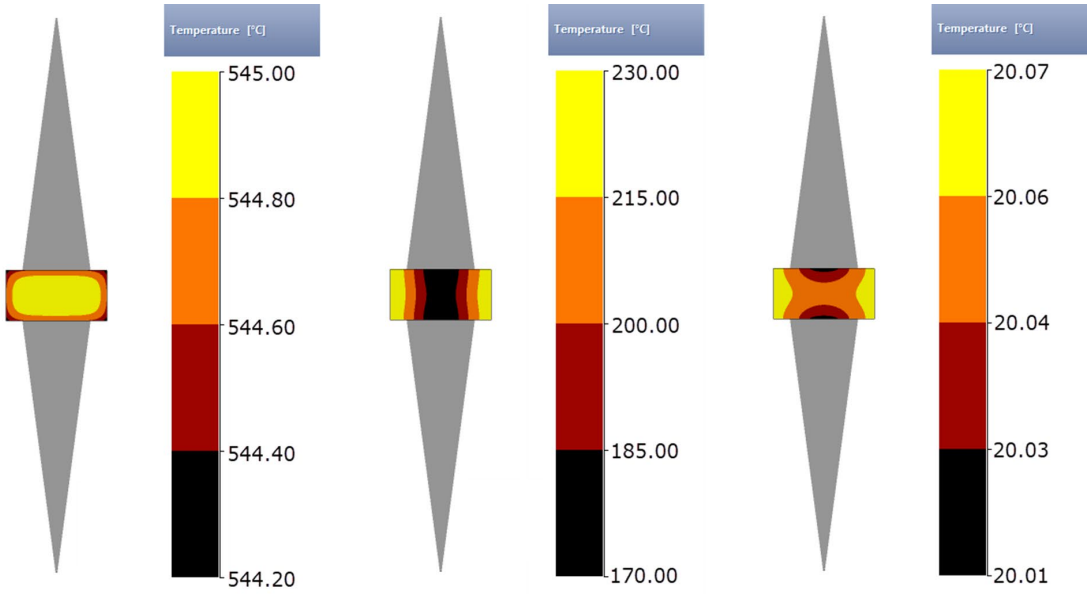

Fig. 7. Temperature distribution at different stages of W3A3-3 simulation process and nozzles alignment. Stages from left to right: beginning, intermediate, final.

The temperature changes for the W3A3-3 mode (indicating a profile speed of 3 m/min) were closely observed at the thermocouple location shown in Fig. 2. Fig. 8a demonstrates that the simulation matches well with the actual experimental results. At a profile speed of 3 m/min, the sample spent about 33 seconds in the quenching system, reducing to around 16.5 seconds at a speed of 6 m/min. However, these results specifically refer to the effective cooling range, focusing on the times when significant temperature changes occurred. Nonetheless, it is worthwhile to plot time with the zero point corresponding to the moment when the sample initiates movement from the oven. This allows for the consideration of temperature drops attributed to internal heat exchange, motion velocity, and cooling intensity before the region of the sample with the thermocouple reaches the quenching box.

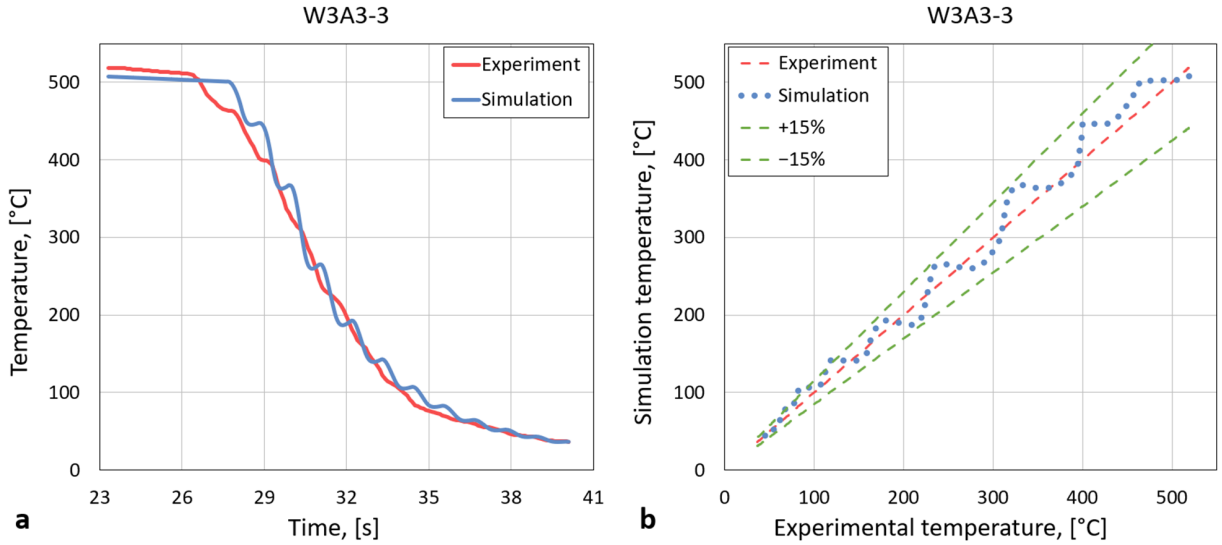

Fig. 8. Comparison of simulation and experiment for W3A3-3 condition: a – temperature-time dependence; b – diagonal graph

To assess simulation accuracy, a statistical analysis was conducted to measure the difference between the simulation and actual values. Figure 8b illustrates this evaluation with a diagonal

graph, showing that all data points fall within the ±15% deviation range from the reference value, confirming the simulation's high accuracy.

The same analysis was applied to the W5A3-3 mode (Fig. 9) and the W5A3-6 mode (Fig. 10), revealing similarly reliable temperature predictions over time. However, there were variations in effective cooling times among these modes. The W3A3-3 mode had the longest effective cooling time range of about 10.3 seconds, the W5A3-6 mode had the shortest range of around 8.2 seconds, and the W5A3-3 mode fell in between with an effective cooling time range of about 9.2 seconds.

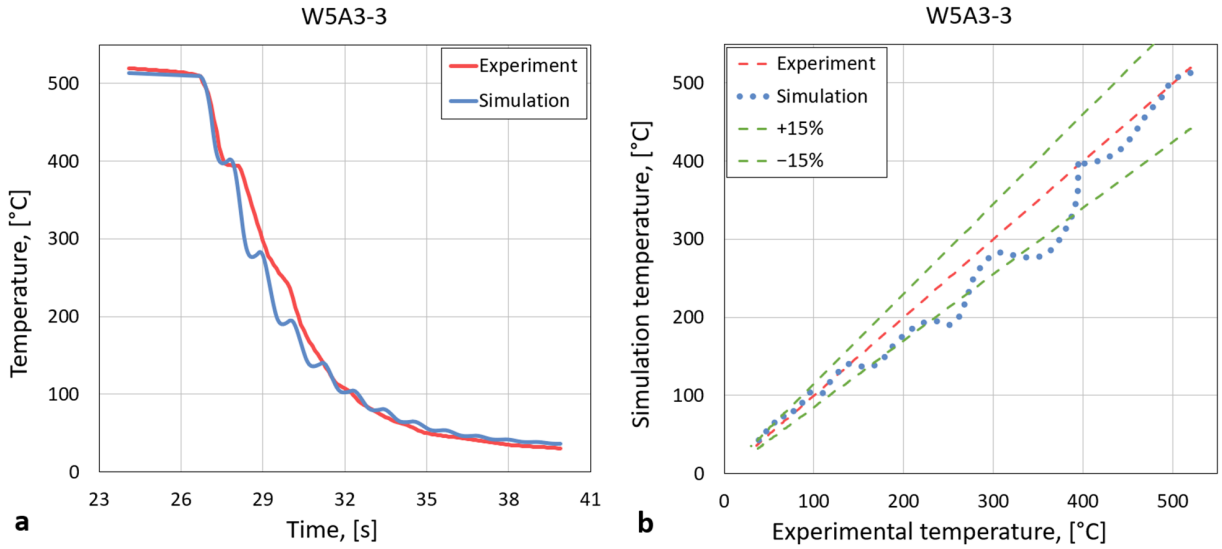

Fig. 9. Comparison of simulation and experiment for W5A3-3 condition: a – temperature-time dependence; b – diagonal graph

It's important to highlight that even when doubling the profile velocity, the slight variation in effective cooling time emphasizes the significant impact of profile thickness on temperature distribution within the profile.

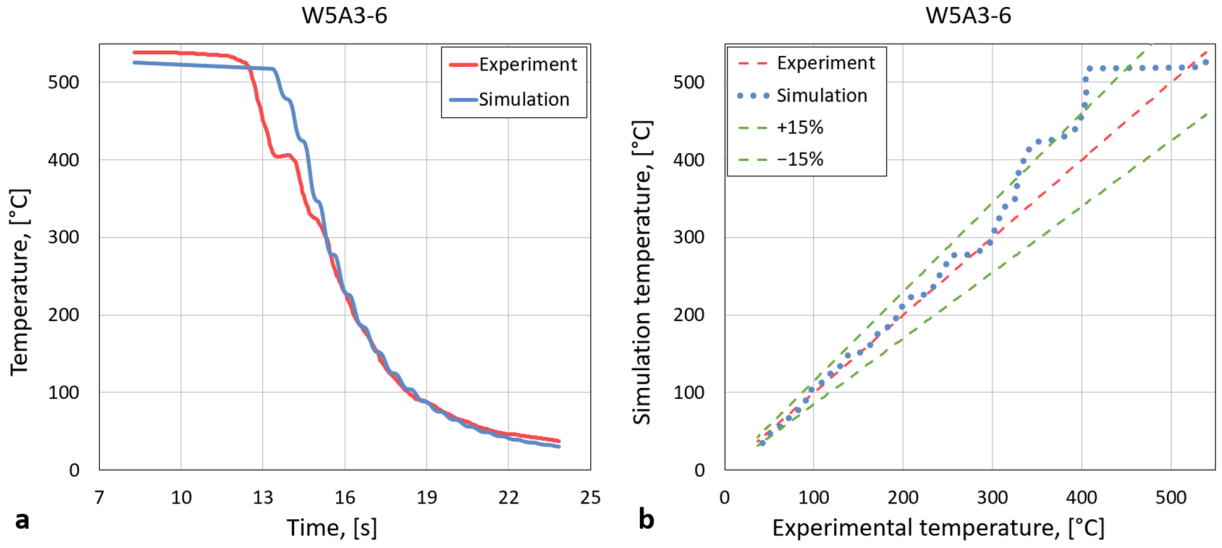

Fig. 10. Comparison of simulation and experiment for W5A3-6 condition: a – temperature-time dependence; b – diagonal graph

To enhance the evaluation of simulation accuracy and provide a clear visual representation, a frequency plot depicting point scatters between the experiment and simulation for various

temperature intervals has been generated for each tested mode (Fig. 11). The histogram illustrates the percentage of measurement points relative to the total number of points, considering the difference between the experiment and simulation within specific temperature difference intervals. Across all tested modes, the majority of points are concentrated in the central row, characterized by the smallest differences. This observation underscores the accuracy of the established relationships between heat transfer coefficient, temperature, and liquid flux density.

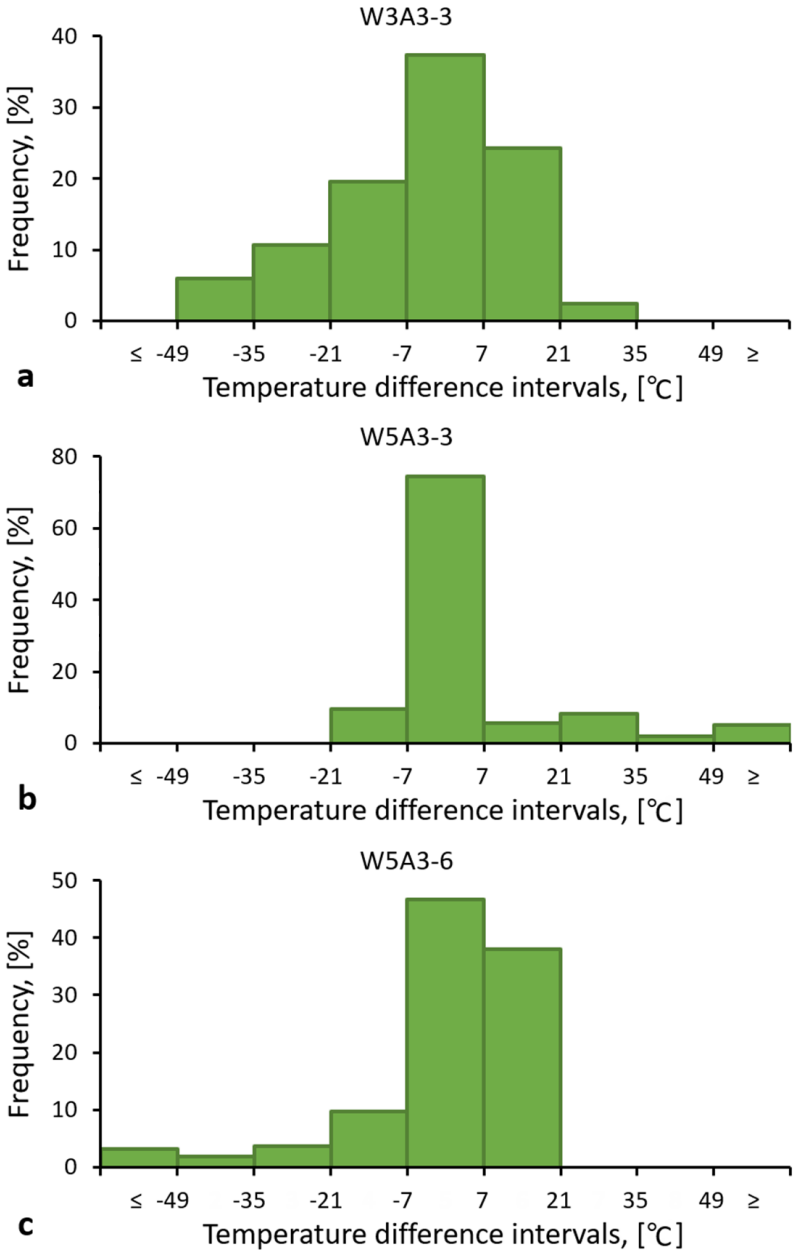

Fig. 11. Frequency histogram of the difference between simulation and experiment for different modes: a – W3A3-3; b – W5A3-3; c – W5A3-6

Summary

This study focused on simulating the cooling processes of extruded profiles, specifically examining the accuracy of numerical simulation in quenching. Employing the QForm UK software, the authors showcased temperature tracing results during quenching, comparing them with laboratory tests.

To enable precise simulation, fundamental dependencies among the heat transfer coefficient, surface temperature, and liquid flux density were established. This involved processing experimental data obtained from laboratory tests closely mirroring industrial conditions.

In conclusion, the study highlights the heightened accuracy of the derived dependencies. This newfound precision allows for the utilization of simulation in optimizing industrial quenching processes for aluminum profiles where water-spray cooling is used.

References

[1] Bikass, S., B. Andersson, A. Pilipenko, and H. P. Langtangen. Simulation of the distortion mechanisms due to non-uniform cooling in the aluminum extrusion process. International journal of thermal sciences 52 (2012) 50-58. https://doi.org/10.1016/j.ijthermalsci.2011.06.002

[2] Negozio, M., Segatori, A., Pelaccia, R., Reggiani, B., & Donati, L. (2024). Experimental investigation and numerical prediction of the peripheral coarse grain (PCG) evolution during the extrusion of different AA6082 aluminum alloy profiles. Materials Characterization, 113723. https://doi.org/10.1016/j.matchar.2024.113723

[3] Tiryakioglu, M., and G. Totten. Quenching aluminum components in water: Problems and alternatives. In Heat Treating: Proceedings of the 18 th Conference, October 12 th-15 th. 1998.

[4] WILLIAMS William M., SANDNES Lise, MA Jun, TRONVOLL Sigmund Arntsønn, WELO Torgeir. Yield stress and work hardening behavior of extruded AA6082 profiles under different homogenisation and extrusion conditions. Materials Research Proceedings 28 (2023) 467-476. https://doi.org/10.21741/9781644902479-51

[5] Osten, Julia, Benjamin Milkereit, Michael Reich, Bin Yang, Armin Springer, Karina Nowak, and Olaf Kessler. Development of precipitation hardening parameters for high strength alloy AA 7068. Materials 13(4) (2020) 918. https://doi.org/10.3390/ma13040918

[6] Mei, R. B., L. Bao, C. S. Li, J. K. Wang, and X. H. Liu. FE analysis of 6063 aluminium profiles with complex cross-section during online quenching processes. Mechanics 21(2) (2015) 99-106. https://doi.org/10.5755/j01.mech.21.2.11733

[7] Kniazkin I., Kulakov I., Shitikov A., Raedt H.-W. Quenching of extruded profiles – finite element simulation as a tool to minimise profile distortion. Aluminium Extrusion Industry, April (2022) 34-35.

[8] Golovko, A. N., D. Rodman, F. Nürnberger, M. Schaper, Ya V. Frolov, and S. M. Beliaiev. Investigation of the Water-Air Cooling Process of the Thick-Walled Extruded Profile Made of Alloy En Aw-6060 on the Output Table. Metallurgical & Mining Industry 4(2) (2012).

[9] Information on https://www.spray.com/-/media/dam/industrial/usa/sales-material/catalog/cat76a-aa_metric.pdf

[10] Abramovich, G. N., Girshovich, T. A., Krasheninnikov, S. I., Sekundov, A. N., and I. P Smirnova. The theory of turbulent jets. Moscow Izdatel Nauka,1984.

[11] Schlichting, H., Gersten, K. Turbulent Free Shear Flows. In: Boundary-Layer Theory. Springer, Berlin, Heidelberg, 2017. https://doi.org/10.1007/978-3-662-52919-5_22

[12] Golovko, O., I. Frolov, D. Rodman, F. Nürnberger, O. Grydin, and M. Schaper. Spray cooling of extruded EN AW-6082 aluminium alloy sheets: spatial heat transfer coefficients. Forschung im Ingenieurwesen 3(78) (2014) 131-137. https://doi.org/10.1007/s10010-014-0181-y